SAND2018-13191J

THE JOURNAL OF PHYSICAL CHEMISTRY Letters

Letter

Cite This: J. Phys. Chem. Lett. 2018, 9, 534−539

pubs.acs.org/JPCL

Radical Thermometers, Thermochemistry, and Photoelectron Spectra: A Photoelectron Photoion Coincidence Spectroscopy Study of the Methyl Peroxy Radical

Krisztina Voronova,[†] Kent M. Ervin,[‡] Krisztián G. Torma,[†] Patrick Hemberger,[§] Andras Bodi,[§] Thomas Gerber,[§] David L. Osborn,[∥] and Bálint Sztáray*[,†]

[†]Department of Chemistry, University of the Pacific, Stockton, California 95211, United States

[‡]Department of Chemistry, University of Nevada, Reno, Reno, Nevada 89557-0216, United States

[§]Paul Scherrer Institute, CH-5232 Villigen PSI, Switzerland

[∥]Combustion Research Facility, Sandia National Laboratories, Livermore, California 94551, United States

Supporting Information

ABSTRACT: We investigated the simplest alkylperoxy radical, CH_3OO, formed by reacting photolytically generated CH_3 radicals with O_2, using the new combustion reactions followed by photoelectron photoion coincidence (CRF-PEPICO) apparatus at the Swiss Light Source. Modeling the experimental photoion mass-selected threshold photoelectron spectrum using Franck−Condon simulations including transitions to triplet and singlet cationic states yielded the adiabatic ionization energy of 10.265 ± 0.025 eV. Dissociative photoionization of CH_3OO generates the CH_3^+ fragment ion at the appearance energy of 11.164 ± 0.010 eV. Combining these two values with $\Delta_f H^\circ_{0K}(CH_3)$ yields $\Delta_f H^\circ_{0K}(CH_3OO)$ = 22.06 ± 0.97 kJ mol^{-1}, reducing the uncertainty of the previously determined value by a factor of 5. Statistical simulation of the CH_3OO breakdown diagram provides a molecular thermometer of the free radical's internal temperature, which we measured to be 330 ± 30 K.

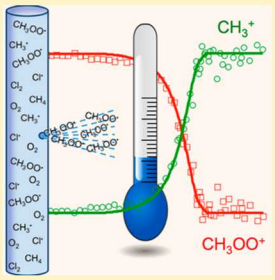

The oxidation of organic molecules, particularly of hydrocarbons, is a crucial process in combustion[1] and atmospheric[2] chemistry. Although decades of research has provided a solid understanding of many reaction mechanisms, there is an ever-increasing need for reliable experimental data to improve the accuracy of predictive models and to extend these models to more complex molecules and reaction conditions.[1] Reactive intermediates, such as alkylperoxy (ROO)[3] and hydroperoxyalkyl (QOOH) radicals, carbonyl oxides (QOO), as well as ketohydroperoxides (OQOOH) play a crucial role in combustion and atmospheric processes.[4] The study of such intermediates is also of fundamental value, providing rich opportunities to understand biradical versus zwitterion reactivity,[5] conformer-resolved chemistry,[6] and autoxidation mechanisms.[4] Contemporary methods to prepare reactive intermediates include jet-stirred reactors, model flames, pyrolysis, discharge, catalytic reactors, laser photolysis, and photolytically initiated chemical reactions.[1,7,8] With the last method, used in the present study, reactive precursors can be selectively formed and collisionally thermalized prior to initiating a chemical reaction (or reactions) at a well-defined time that generates the desired reactive intermediate.

Tunable vacuum ultraviolet synchrotron radiation combined with multiplexed photoionization mass spectrometry (PI-MS) is now a well-proven universal detection tool of such elusive molecules such as Criegee intermediates and QOOH radicals.[3,9−11] In this method, after a mixture of molecules is separated by mass-to-charge (m/z) ratio, the remaining isobaric species (that is, isomers) can often be distinguished by measuring the photoionization spectrum (ion intensity vs photon energy). Photoelectron photoion coincidence spectroscopy (PEPICO) offers superior selectivity by also recording the photoelectron spectrum (e.g., threshold photoelectron intensity vs photon energy).[12] Detecting photoions and photoelectrons in coincidence allows the assignment of each electron to its corresponding photoion and, consequently, to the neutral species that created it. Thus, PEPICO allows us to record photoelectron spectra for each m/z ratio from a complex gas mixture, effectively combining the m/z mass selection and sensitivity of mass spectrometry with the isomer selectivity of photoelectron spectroscopy (PES), making PEPICO a promising quantitative time-, space-, and isomer-resolved analysis tool.[12−14] Therefore, after demonstrating its utility in proof-of-concept experiments,[12] we have recently designed and built a new experimental apparatus, which we named combustion reactions followed by photoelectron photoion coincidence (CRF-PEPICO).[13,14]

Beyond its advantages for isomer identification, PEPICO enables measurement of thermochemical data (such as bond energies) with high accuracy[15−17] by inducing unimolecular dissociation of the photoion. Recent improvements to light

Received: November 27, 2017
Accepted: December 31, 2017
Published: December 31, 2017

DOI: 10.1021/acs.jpclett.7b03145
J. Phys. Chem. Lett. 2018, 9, 534−539

sources, PEPICO electron and ion optics, and statistical thermodynamics modeling have generated new interest in using PEPICO for high-accuracy thermochemical measurements[18−23] and extended its applicability to free radicals.[24−28] However, the difficulty of generating high densities of free radicals has made it challenging to obtain high-quality fractional photoion abundance (breakdown) curves of these molecules, inhibiting accurate thermochemical studies of reactive intermediates. Therefore, dissociative ionization thresholds were obtained only from incomplete and low-resolution PEPICO data for the ethyl, propargyl,[29] and allyl[30] radicals. Recently, some of us have investigated the cyclopropenylidene c-C_3H_2 carbene and were able to collect a full breakdown diagram, albeit with low signal-to-noise ratio and significant thermal broadening,[31] both of which reduce the accuracy of the determined dissociation energetics.

Methylperoxy (CH_3OO), the simplest alkylperoxy radical, has been studied extensively both experimentally[3,32,33] and with quantum-chemical methods.[34,35] The neutral radical has a staggered conformation,[34] and its cation is one of the very few bound alkylperoxy cations.[3] The photoionization spectrum (also called photoionization efficiency curve, PIE) of CH_3OO was measured by Meloni et al.[3] using time-resolved multiplexed photoionization mass spectrometry. From this experiment, the adiabatic ionization energy of CH_3OO was determined to be 10.33 ± 0.05 eV, and the threshold to dissociative ionization to CH_3^+ was reported as 11.16 ± 0.05 eV.

In this work, we present the photoion mass-selected threshold photoelectron spectrum (ms-TPES) of the methylperoxy radical, recorded on the new CRF-PEPICO spectrometer,[14] along with a detailed Franck−Condon (FC) analysis to refine its experimental adiabatic ionization energy. We have also studied the fragmentation of energy-selected methylperoxy cations and were able to record a room-temperature breakdown diagram with high signal-to-noise ratio for a transient species.

The CRF-PEPICO spectrometer[14] combines a room-temperature reactive intermediate source, a 57.4 cm long, 1.05 cm I.D. side-sampled quartz flow tube reactor, with a high-resolution double-imaging PEPICO spectrometer, coupled to the VUV beamline of the Swiss Light Source. The methylperoxy radicals were produced according to the following scheme:

$$Cl_2 \xrightarrow{355\ nm} 2Cl \quad (1)$$

$$Cl + CH_4 \rightarrow CH_3 + HCl \quad (2)$$

$$CH_3 + O_2 + M \rightarrow CH_3OO + M \quad (3)$$

During the experiment, metered flows of methane, Cl_2 gas (2% mixture in Ar), and excess reactant O_2 were mixed in situ at the entrance of the reactor flow tube at a total pressure of 1.1 mbar. The concentrations of chlorine and oxygen were optimized to maximize the CH_3OO^+ ion abundance. A pulsed Nd:YAG laser (355 nm, 80 mJ/pulse, 20 Hz repetition rate) propagated down the reactor tube, and the reaction products were sampled into the ionization region through a 400 μm pinhole at the halfway point of the flow tube. Tunable VUV synchrotron radiation intersected the effusive beam of the neutral gas sample, and the resulting photoelectrons and photoions were extracted in opposite directions with a constant electric field of 125 V cm^{-1}. Both electrons and ions were imaged onto position-sensitive delay-line detectors, fulfilling velocity map imaging and, for the ions, also Wiley−McLaren space-focusing conditions. The setup offers better than 1 meV kinetic energy resolution at threshold[14] to record mass-selected threshold photoelectron spectra as well as breakdown curves for energy-selected precursor ions. The raw data of electron and ion detection times and positions as well as the laser trigger times can be analyzed in a number of ways. After the contribution of high kinetic energy electrons is subtacted,[36] the multidimensional data set yields (a) threshold ionization mass spectra, (b) photoion mass-selected threshold photoelectron spectra, and (c) reaction kinetics traces by plotting the coincidence intensity of a particular m/z ratio against kinetic time. The kinetic time profiles of CH_3 and CH_3OO radicals are shown in Figure 1. The methyl radical signal starts to decay 2 ms after the laser pulse, as methyl peroxy radicals are formed and subsequently decay.

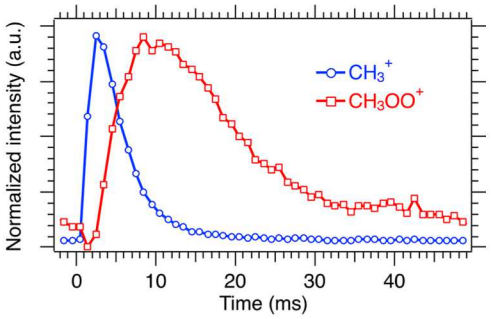

Figure 1. CH_3^+ and CH_3OO^+ kinetic traces in the presence of oxygen, integrated over the 10.24−11.31 eV photon energy range.

Because the CH_3OO^+ parent ion begins to dissociate by O_2 loss into the methyl cation at 10.98 eV (4% daughter ion intensity, according to the model fitted to the breakdown curve, vide infra), the threshold photoelectron spectrum of the CH_3OO radical is obtained by summing the m/z = 47 and m/z = 15 threshold coincidence signals (see Figure 2). One needs to

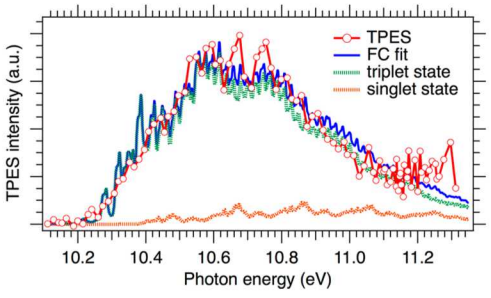

Figure 2. Experimental threshold photoelectron spectrum (red open circles) and the Franck−Condon simulation (blue line) that provided the best overall fit to the experimental data. [Other simulations are described in detail in the Supporting Information, leading to the final AIE(CH_3OO) = 10.265 ± 0.025 eV.] The triplet and singlet states are shown with dashed green and orange lines, respectively.

be careful, however, as this latter signal could also arise from threshold photoionization of the methyl radical. In that case, because the methyl and methylperoxy radicals' kinetic traces are very different, the two contributions to m/z = 15 signal could be separated by integrating over the appropriate kinetic time intervals, utilizing the third dimension of the PEPICO data. However, this approach was not needed because, serendipitously, the threshold photoionization cross section of the

DOI: 10.1021/acs.jpclett.7b03145
J. Phys. Chem. Lett. 2018, 9, 534−539

methyl radical is negligible above 10.98 eV,[24] and the m/z = 15 signal is solely due to dissociative photoionization of CH_3OO above this energy. Therefore, the entire kinetic time interval up to the next laser pulse could be used to plot the TPES of CH_3OO, which is shown in Figure 2, together with results of the Franck−Condon simulations.

Starting in the neutral CH_3OO $\tilde{X}(^2A'')$ state, our highest-level electronic structure calculations at the CCSD(T)/aug-cc-pVQZ//CCSD/aug-cc-pVTZ level of theory predict that removal of an in-plane (a′) electron from a doubly occupied orbital creates the ground-state cation CH_3OO^+ $\tilde{X}^+(^3A'')$, with a zero-point corrected ionization energy of 10.21 eV. Removal of the electron from the singly occupied out-of-plane (a″) orbital generates the excited-state singlet CH_3OO^+ $\tilde{a}^+(^1A')$, with an ionization energy of 10.37 eV (Table S1). Both ionization energies are in good agreement with previous calculations.[3] Franck−Condon calculations[37] elucidate the vibrational transitions underpinning the photoelectron spectrum and are described in detail in the Supporting Information. In brief, the harmonic oscillator approximation is used for all vibrational modes except the CH_3−OO torsional mode, which is treated as a hindered rotor in the neutral and the cationic states. Geometries and harmonic frequencies at the CCSD/aug-cc-pVTZ level were used for all normal modes other than the torsional mode. Relaxed torsional potential energy scans at the B3LYP/aug-cc-pVTZ level were scaled to barrier heights at the CCSD(T)/aug-cc-pVQZ//CCSD/aug-cc-pVTZ level then fit to a cosine power series. Energy levels and wave functions were obtained by numerically solving the one-dimensional hindered rotor Schrödinger equation within a free-rotor basis set.

Considering first the totally symmetric vibrational modes, there is substantial geometry change between the neutral and CH_3OO^+ $\tilde{X}^+(^3A'')$ in four of the totally symmetric normal modes, most importantly in the CH_3−OO stretch and the COO bending mode.[3] Transitions to the excited-state singlet involve removal of an electron in the singly occupied a″ orbital on the terminal oxygen atom and hence cause less geometry change in the C−O bond length and the ∠CCO compared to forming the ground-state triplet from the neutral. However, the nontotally symmetric CH_3−OO torsional mode behaves quite differently when comparing the two cationic states.

In the torsional coordinate, both neutral CH_3OO and the ground-state CH_3OO^+ $\tilde{X}^+(^3A'')$ have a staggered equilibrium geometry, whereas the CH_3OO^+ $\tilde{a}^+(^1A')$ excited state is at a potential maximum in the staggered configuration. These geometries imply good FC overlap in the torsional coordinate for transitions to the ground-state cation but poor FC overlap to the excited-state cation along the torsional coordinate until energy in the torsional coordinate is near the 459 cm^{-1} barrier to singlet-state internal rotation. This geometry change shifts the beginning of the FC envelope approximately 459 cm^{-1} (57 meV) higher than the adiabatic ionization energy of CH_3OO^+ $\tilde{a}^+(^1A')$.

The experimental spectrum is less structured than either the triplet- or singlet-state simulation, partly because the 15 meV spacing of the experimental data is too sparse to resolve narrow peaks. However, the lack of resolved structure and the calculated small triplet−singlet energy spacing of 0.15 eV (calculated at the CCSD(T)/aug-cc-pVQZ//CCSD/aug-cc-pVTZ level of theory; other high-level calculations place this spacing between 0.12 and 0.16 eV, see Table S1) imply that the two states overlap to create a congested profile. Therefore, no definitive assignment of the origin based on resolved vibrational transitions could be made. Instead, the combined simulated triplet and singlet bands were fitted to the overall envelope, using the sample temperature determined from the breakdown curve (vide infra). Keeping the vibrational frequencies, geometry displacements, and torsional parameters as fixed parameters and varying the ionization energy, triplet−singlet energy splitting, and the relative transition intensities of the two states (as described in the Supporting Information, see Figures S4−S6), gives an adiabatic ionization energy of AIE = 10.265 ± 0.025 eV and a triplet−singlet spacing of 0.15 eV.

As mentioned earlier, because the methyl radical has no Franck−Condon transitions in the photon energy range of the CH_3OO to CH_3^+ dissociative photoionization, we could obtain a remarkably clean breakdown diagram, plotted in Figure 3.

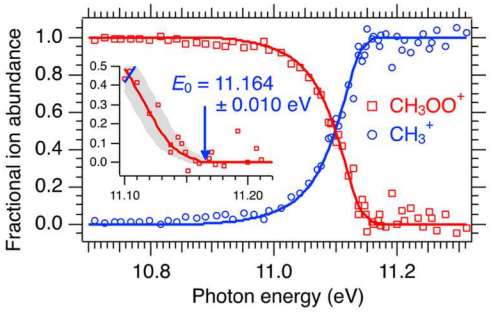

Figure 3. Breakdown diagram for CH_3OO^+. Open symbols are experimentally measured ion abundances and lines are the statistical rate theory modeling of the data.

Because the last discernible methyl radical TPES transition[24] is just below 10.98 eV, only the data points above this photon energy were used in the modeling of the breakdown curve to determine the 0 K appearance energy of the methyl cation from CH_3OO^+ dissociation.

As evidenced by the symmetric and sharp m/z = 15 fragment ion peak in the PEPICO TOF mass spectrum (Figure S1), O_2 loss from CH_3OO^+ is fast on the time scale of the experiment. Therefore, the breakdown diagram depends only on the 0 K appearance energy, E_0, and the thermal energy distribution of the sample, calculated using harmonic vibrational frequencies from the quantum-chemical calculations (vide infra). When the cationic potential energy well is deep enough to support the thermal energy distribution of the neutral, the breakdown diagram can be used effectively as a molecular thermometer.[38] We treated the model temperature as a fitting parameter; it optimized to 330 ± 30 K (see Figure S7). This best-fit temperature was also used in the Franck−Condon simulations of the TPES.

Because hydrogen abstraction from methane by a chlorine atom (reaction 2) is close to thermoneutral, methyl radicals will be thermally equilibrated before participating in reaction 3. However, the reaction enthalpy of oxygen addition to methyl is −133.8 ± 0.5 kJ mol^{-1},[39] orders of magnitude more than the internal energy of equilibrated methyl peroxy at room temperature. Because the pressure drop between the reactor tube and the ionization point is relatively small, we expect the resulting Joule−Thompson cooling to be negligible, so that the temperature obtained from the breakdown curve may be used to quantify the temperature of the CH_3OO radical in the reactor. The 330 ± 30 K temperature supports our conclusion that CH_3OO is almost completely relaxed to room temperature by collisions in the reactor. Although in this experiment we

DOI: 10.1021/acs.jpclett.7b03145
J. Phys. Chem. Lett. 2018, 9, 534−539

have insufficient signal-to-noise to determine CH_3OO temperature as a function of time after the photolysis pulse, in principle this is also possible, enabling us to explicitly monitor collisional cooling by fitting the breakdown diagram as a function of kinetic time. We anticipate that this approach will be valuable both for confirming thermal equilibrium of radicals and also, in other cases, to identify nonequilibrated energy distributions in investigations of nonthermal reactions, which are of increasing interest in the atmospheric and combustion communities.[4,40]

Although the methyl peroxy breakdown curve could be modeled equally well with or without including the hindered methyl rotation, the inclusion of the hindered rotor was found to reproduce the experimental breakdown curve much better in an earlier study on methanol.[41] Therefore, we included a Pitzer hindered rotor in the energy distribution model for neutral CH_3OO, with a rotational barrier height of 336 cm^{-1} [average of values shown in Table S1, except B3LYP/6-311++G-(2df,2p)]. Fitting the model to the experimental breakdown curve yields a 0 K appearance energy of E_0 = 11.164 ± 0.010 eV. This value agrees with the 11.16 ± 0.05 eV determination of Meloni et al. but improves its uncertainty by a factor of 5.[3]

Through a thermochemical cycle (Figure 4), our 0 K appearance energy connects the heat of formation of CH_3OO

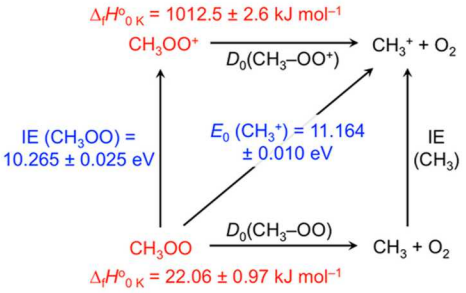

Figure 4. Positive ion thermochemical cycle of the methylperoxy system. The ionization energy of CH_3OO and the appearance energy of the CH_3^+ daughter ion, highlighted in blue, are experimentally measured in this work.

with that of CH_3^+. The latter is listed as $\Delta_f H^\circ_{0K}$ (CH_3^+) = 1099.243 ± 0.078 kJ mol^{-1} in the newest release of the Active Thermochemical Tables (ATcT),[39] from which we derive $\Delta_f H^\circ_{0K}$ (CH_3OO) = 22.06 ± 0.97 kJ mol^{-1}. This value is in agreement with both the 22.4 ± 5 kJ mol^{-1} of Meloni et al.[3] and 22.29 ± 0.49 kJ mol^{-1} as reported in version 1.122 of the ATcT.[39] Using our methylperoxy ionization energy of 10.265 ± 0.025 eV (990.44 ± 2.41 kJ mol^{-1}), the heat of formation of the cation can now be calculated to be $\Delta_f H^\circ_{0K}(CH_3OO^+)$ = 1012.5 ± 2.6 kJ mol^{-1}. This value is again in excellent agreement with 1012.2 ± 2.0 kJ mol^{-1}, as listed in ATcT, and overlaps with the uncertainty limits of 1019 ± 7 kJ mol^{-1}, as derived by Meloni et al.[3]

The thermochemical cycle in Figure 4 also yields neutral and ionic bond energies. The ionization energy of the methyl radical, IE(CH_3) = 9.83891 ± 0.00019 eV (949.311 ± 0.018 kJ mol^{-1},)[42] and the appearance energy of $CH_3OO \rightarrow CH_3^+ + O_2 + e^-$ yields $D_0(CH_3–OO)$ = 127.85 ± 0.97 kJ mol^{-1}. Subtracting the hereby determined IE of CH_3OO from the PEPICO appearance energy yields the CH_3^+–OO bond energy in the cation as 86.7 ± 2.6 kJ mol^{-1}.

To conclude, the new double-imaging CRF-PEPICO apparatus[14] has been used to record the first threshold photoelectron spectrum of the methyl peroxy radical. This prototypical free radical was formed by hydrogen atom abstraction from methane with photolytically generated chlorine atoms and the subsequent reaction with oxygen molecules. Together with Franck–Condon simulations including a hindered rotor treatment, the TPES allowed us to extract the adiabatic ionization energy of the methyl peroxy radical. Oxygen molecule loss by dissociative ionization from the internal energy selected methyl peroxy cations was also investigated. Statistical energy distribution modeling of the experimental breakdown curve yielded the first 0 K appearance energy measured with sub-kilojoule per mole accuracy for a reactive intermediate. Combining these experimental data allowed us to determine accurate neutral and ionic methyl–peroxy bond energies, showing how the well-proven technique of PEPICO combined with new inlet systems to generate radicals opens up the field of positive ion cycles to such important reactive intermediates, contributing to the thermochemistry of radicals. The derived heats of formation agree well with data from the latest version of the Active Thermochemical Tables. More importantly, including the experimental 0 K methyl cation appearance energy in ATcT will likely reduce the uncertainty in the heats of formation of a number of connected species.[39] Finally, we show that modeling a high S/N breakdown curve can also serve as molecular thermometer of free radicals, which can be used to monitor whether these species have reached thermal equilibrium, a contentious issue in kinetics studies.

■ ASSOCIATED CONTENT

Supporting Information

The Supporting Information is available free of charge on the ACS Publications website at DOI: 10.1021/acs.jpclett.7b03145.

PEPICO time-of-flight mass spectra, detailed description of the Franck–Condon simulations, and additional fits to the threshold photoelectron spectrum of CH_3OO. (PDF)

■ AUTHOR INFORMATION

Corresponding Author

*E-mail: bsztaray@pacific.edu.

ORCID

Patrick Hemberger: 0000-0002-1251-4549
Andras Bodi: 0000-0003-2742-1051
Bálint Sztáray: 0000-0002-0333-0000

Notes

The authors declare no competing financial interest.

■ ACKNOWLEDGMENTS

This work has been funded by the National Science Foundation (Grant No. CHE-1665464) and by the Swiss Federal Office for Energy (BFE Contract No. SI/501269-01). This material is based upon work supported by the U.S. Department of Energy, Office of Science, Office of Basic Energy Sciences. Sandia National Laboratories is a multimission laboratory managed and operated by National Technology and Engineering Solutions of Sandia, LLC., a wholly owned subsidiary of Honeywell International, Inc., for the U.S. Department of Energy's National Nuclear Security Administration under contract DE-NA0003525. Experiments were performed at the

DOI: 10.1021/acs.jpclett.7b03145
J. Phys. Chem. Lett. 2018, 9, 534–539

VUV (x04db) beamline at the Swiss Light Source located at the Paul Scherrer Institute.

REFERENCES

(1) Zádor, J.; Taatjes, C. A.; Fernandes, R. X. Kinetics of Elementary Reactions in Low-Temperature Autoignition Chemistry. *Prog. Energy Combust. Sci.* **2011**, *37*, 371−421.

(2) Ehn, M.; Thornton, J. A.; Kleist, E.; Sipila, M.; Junninen, H.; Pullinen, I.; Springer, M.; Rubach, F.; Tillmann, R.; Lee, B.; et al. A Large Source of Low-Volatility Secondary Organic Aerosol. *Nature* **2014**, *506*, 476−479.

(3) Meloni, G.; Zou, P.; Klippenstein, S. J.; Ahmed, M.; Leone, S. R.; Taatjes, C. A.; Osborn, D. L. Energy-Resolved Photoionization of Alkylperoxy Radicals and the Stability of Their Cations. *J. Am. Chem. Soc.* **2006**, *128*, 13559−13567.

(4) Osborn, D. L. Reaction Mechanisms on Multiwell Potential Energy Surfaces in Combustion (and Atmospheric) Chemistry. *Annu. Rev. Phys. Chem.* **2017**, *68*, 233−260.

(5) Taatjes, C. A. Criegee Intermediates: What Direct Production and Detection Can Teach Us About Reactions of Carbonyl Oxides. *Annu. Rev. Phys. Chem.* **2017**, *68*, 183−207.

(6) Taatjes, C. A.; Welz, O.; Eskola, A. J.; Savee, J. D.; Scheer, A. M.; Shallcross, D. E.; Rotavera, B.; Lee, E. P. F.; Dyke, J. M.; Mok, D. K. W.; et al. Direct Measurements of Conformer-Dependent Reactivity of the Criegee Intermediate CH_3CHOO. *Science* **2013**, *340*, 177−180.

(7) Battin-Leclerc, F. Detailed Chemical Kinetic Models for the Low-Temperature Combustion of Hydrocarbons with Application to Gasoline and Diesel Fuel Surrogates. *Prog. Energy Combust. Sci.* **2008**, *34*, 440−498.

(8) Hemberger, P.; Custodis, V. B. F.; Bodi, A.; Gerber, T.; van Bokhoven, J. A. Understanding the Mechanism of Catalytic Fast Pyrolysis by Unveiling Reactive Intermediates in Heterogeneous Catalysis. *Nat. Commun.* **2017**, *8*, 15946.

(9) Osborn, D. L.; Zou, P.; Johnsen, H.; Hayden, C. C.; Taatjes, C. A.; Knyazev, V. D.; North, S. W.; Peterka, D. S.; Ahmed, M.; Leone, S. R. The Multiplexed Chemical Kinetic Photoionization Mass Spectrometer: a New Approach to Isomer-Resolved Chemical Kinetics. *Rev. Sci. Instrum.* **2008**, *79*, 104103.

(10) Welz, O.; Savee, J. D.; Osborn, D. L.; Vasu, S. S.; Percival, C. J.; Shallcross, D. E.; Taatjes, C. A. Direct Kinetic Measurements of Criegee Intermediate (CH_2OO) Formed by Reaction of CH_2I with O_2. *Science* **2012**, *335*, 204−207.

(11) Savee, J. D.; Papajak, E.; Rotavera, B.; Huang, H.; Eskola, A. J.; Welz, O.; Sheps, L.; Taatjes, C. A.; Zádor, J.; Osborn, D. L. Direct Observation and Kinetics of a Hydroperoxyalkyl Radical (QOOH). *Science* **2015**, *347*, 643−646.

(12) Bodi, A.; Hemberger, P.; Osborn, D. L.; Sztáray, B. Mass-Resolved Isomer-Selective Chemical Analysis with Imaging Photoelectron Photoion Coincidence Spectroscopy. *J. Phys. Chem. Lett.* **2013**, *4*, 2948−2952.

(13) Osborn, D. L.; Hayden, C. C.; Hemberger, P.; Bodi, A.; Voronova, K.; Sztáray, B. Breaking Through the False Coincidence Barrier in Electron-Ion Coincidence Experiments. *J. Chem. Phys.* **2016**, *145*, 164202.

(14) Sztáray, B.; Voronova, K.; Torma, K. G.; Covert, K. J.; Bodi, A.; Hemberger, P.; Gerber, T.; Osborn, D. L. CRF-PEPICO: Double Velocity Map Imaging Photoelectron Photoion Coincidence Spectroscopy for Reaction Kinetics Studies. *J. Chem. Phys.* **2017**, *147*, 013944.

(15) Bodi, A.; Csontos, J.; Kállay, M.; Borkar, S.; Sztáray, B. On the Protonation of Water. *Chem. Sci.* **2014**, *5*, 3057−3063.

(16) Bodi, A.; Baer, T.; Wells, N. K.; Fakhoury, D.; Klecyngier, D.; Kercher, J. P. Controlling Tunnelling in Methane Loss from Acetone Ions by Deuteration. *Phys. Chem. Chem. Phys.* **2015**, *17*, 28505−28509.

(17) Steglich, M.; Custodis, V. B. F.; Trevitt, A. J.; daSilva, G.; Bodi, A.; Hemberger, P. Photoelectron Spectrum and Energetics of the meta-Xylylene Diradical. *J. Am. Chem. Soc.* **2017**, *139*, 14348−14351.

(18) Bodi, A.; Sztáray, B.; Baer, T.; Johnson, M.; Gerber, T. Data Acquisition Schemes for Continuous Two-Particle Time-Of-Flight Coincidence Experiments. *Rev. Sci. Instrum.* **2007**, *78*, 084102.

(19) Garcia, G. A.; Soldi-Lose, H.; Nahon, L. A Versatile Electron-Ion Coincidence Spectrometer for Photoelectron Momentum Imaging and Threshold Spectroscopy on Mass Selected Ions Using Synchrotron Radiation. *Rev. Sci. Instrum.* **2009**, *80*, 023102.

(20) Bodi, A.; Johnson, M.; Gerber, T.; Gengeliczki, Z.; Sztáray, B.; Baer, T. Imaging Photoelectron Photoion Coincidence Spectroscopy with Velocity Focusing Electron Optics. *Rev. Sci. Instrum.* **2009**, *80*, 034101.

(21) Tang, X.; Zhou, X.; Niu, M.; Liu, S.; Sun, J.; Shan, X.; Liu, F.; Sheng, L. A Threshold Photoelectron-Photoion Coincidence Spectrometer with Double Velocity Imaging Using Synchrotron Radiation. *Rev. Sci. Instrum.* **2009**, *80*, 113101.

(22) Sztáray, B.; Bodi, A.; Baer, T. Modeling Unimolecular Reactions in Photoelectron Photoion Coincidence Experiments. *J. Mass Spectrom.* **2010**, *45*, 1233−1245.

(23) Bodi, A.; Hemberger, P.; Gerber, T.; Sztáray, B. A New Double Imaging Velocity Focusing Coincidence Experiment: i^2PEPICO. *Rev. Sci. Instrum.* **2012**, *83*, 083105.

(24) Kruger, J.; Garcia, G. A.; Felsmann, D.; Moshammer, K.; Lackner, A.; Brockhinke, A.; Nahon, L.; Kohse-Hoinghaus, K. Photoelectron-Photoion Coincidence Spectroscopy for Multiplexed Detection of Intermediate Species in a Flame. *Phys. Chem. Chem. Phys.* **2014**, *16*, 22791−22804.

(25) Garcia, G. A.; Tang, X.; Gil, J.-F.; Nahon, L.; Ward, M.; Batut, S.; Fittschen, C.; Taatjes, C. A.; Osborn, D. L.; Loison, J.-C. Synchrotron-Based Double Imaging Photoelectron/Photoion Coincidence Spectroscopy Of Radicals Produced in a Flow Tube: OH and OD. *J. Chem. Phys.* **2015**, *142*, 164201.

(26) Zhu, Y.; Wu, X.; Tang, X.; Wen, Z.; Liu, F.; Zhou, X.; Zhang, W. Synchrotron Threshold Photoelectron Photoion Coincidence Spectroscopy of Radicals Produced in a Pyrolysis Source: the Methyl Radical. *Chem. Phys. Lett.* **2016**, *664*, 237−241.

(27) Baer, T.; Tuckett, R. P. Advances in Threshold Photoelectron Spectroscopy (TPES) and Threshold Photoelectron Photoion Coincidence (TPEPICO). *Phys. Chem. Chem. Phys.* **2017**, *19*, 9698−9723.

(28) Reusch, E.; Holzmeier, F.; Constantinidis, P.; Hemberger, P.; Fischer, I. Isomer-Selective Generation and Spectroscopic Characterization of Picolyl Radicals. *Angew. Chem., Int. Ed.* **2017**, *56*, 8000−8003.

(29) Schüßler, T.; Roth, W.; Gerber, T.; Alcaraz, C.; Fischer, I. The VUV Photochemistry of Radicals: C_3H_3 and C_2H_5. *Phys. Chem. Chem. Phys.* **2005**, *7*, 819−825.

(30) Fischer, I.; Schüßler, T.; Deyerl, H.-J.; Elhanine, M.; Alcaraz, C. Photoionization and Dissociative Photoionization of the Allyl Radical, C_3H_5. *Int. J. Mass Spectrom.* **2007**, *261*, 227−233.

(31) Holzmeier, F.; Fischer, I.; Kiendl, B.; Krueger, A.; Bodi, A.; Hemberger, P. On the Absolute Photoionization Cross Section and Dissociative Photoionization of Cyclopropenylidene. *Phys. Chem. Chem. Phys.* **2016**, *18*, 9240−9247.

(32) Blanksby, S. J.; Ramond, T. M.; Davico, G. E.; Nimlos, M. R.; Kato, S.; Bierbaum, V. M.; Lineberger, W. C.; Ellison, G. B.; Okumura, M. Negative-Ion Photoelectron Spectroscopy, Gas-Phase Acidity, and Thermochemistry of the Peroxyl Radicals CH_3OO and CH_3CH_2OO. *J. Am. Chem. Soc.* **2001**, *123*, 9585−9596.

(33) Hsu, K.-H.; Huang, Y.-H.; Lee, Y.-P.; Huang, M.; Miller, T. A.; McCoy, A. B. Manifestations of Torsion-CH Stretch Coupling in the Infrared Spectrum of CH_3OO. *J. Phys. Chem. A* **2016**, *120*, 4827−4837.

(34) Just, G. M. P.; McCoy, A. B.; Miller, T. A. Effect of Methyl Rotation on the Electronic Spectrum of the Methyl Peroxy Radical. *J. Chem. Phys.* **2007**, *127*, 044310.

(35) Copan, A. V.; Schaefer, H. F.; Agarwal, J. Examining the Ground and First Excited States of Methyl Peroxy Radical with High-Level Coupled-Cluster Theory. *Mol. Phys.* **2015**, *113*, 2992−2998.

DOI: 10.1021/acs.jpclett.7b03145
J. Phys. Chem. Lett. 2018, 9, 534−539

(36) Sztáray, B.; Baer, T. Suppression of Hot Electrons in Threshold Photoelectron Photoion Coincidence Spectroscopy Using Velocity Focusing Optics. *Rev. Sci. Instrum.* **2003**, *74*, 3763−3768.
(37) Ervin, K. M.; Ramond, T. M.; Davico, G. E.; Schwartz, R. L.; Casey, S. M.; Lineberger, W. C. Naphthyl Radical: Negative Ion Photoelectron Spectroscopy, Franck−Condon Simulation, and Thermochemistry. *J. Phys. Chem. A* **2001**, *105*, 10822−10831.
(38) Harvey, J.; Tuckett, R. P.; Bodi, A. A Halomethane Thermochemical Network from iPEPICO Experiments and Quantum Chemical Calculations. *J. Phys. Chem. A* **2012**, *116*, 9696−9705.
(39) Ruscic, B.; Bross, D. H. Active Thermochemical Tables (ATcT) values based on ver. 1.122 of the Thermochemical Network (2016); available at ATcT.anl.gov (accessed October 10, 2017).
(40) Glowacki, D. R.; Lockhart, J.; Blitz, M. A.; Klippenstein, S. J.; Pilling, M. J.; Robertson, S. H.; Seakins, P. W. Interception of Excited Vibrational Quantum States by O_2 in Atmospheric Association Reactions. *Science* **2012**, *337*, 1066−1069.
(41) Borkar, S.; Sztáray, B.; Bodi, A. Dissociative Photoionization Mechanism of Methanol Isotopologues (CH_3OH, CD_3OH, CH_3OD and CD_3OD) by iPEPICO: Energetics, Statistical and Non-Statistical Kinetics and Isotope Effects. *Phys. Chem. Chem. Phys.* **2011**, *13*, 13009−13020.
(42) Schulenburg, A. M.; Alcaraz, C.; Grassi, G.; Merkt, F. Rovibrational Photoionization Dynamics of Methyl and its Isotopomers Studied by High-Resolution Photoionization and Photoelectron Spectroscopy. *J. Chem. Phys.* **2006**, *125*, 104310.

DOI: 10.1021/acs.jpclett.7b03145
J. Phys. Chem. Lett. 2018, 9, 534−539